

Optimization-free super-oscillatory lens using phase and amplitude masks

Kun Huang¹, Huapeng Ye¹, Jinghua Teng², Swee Ping Yeo¹, Boris Luk'yanchuk^{3*}, and Cheng-Wei Qiu^{1*}

*Email: eleqc@nus.edu.sg; Tel: (65) 65162559; Fax: (65) 67791103

¹Department of Electrical and Computer Engineering, National University of Singapore, 4 Engineering Drive 3, Singapore 117583, Singapore

²Institute of Materials Research and Engineering, Agency for Science, Technology and Research, Singapore 117602, Singapore

³Data Storage Institute, Agency for Science, Technology and Research, 5 Engineering Drive 1, Singapore 117608, Singapore

Supplementary Materials for Design Procedure and Criteria

1. The intensity and phase of light passing through a single belt with its radius r_0 and width Δr . In Fig. 1, we show the sketch of the diffraction of a belt with radius r_0 and width Δr . The angle between the ray emitting from the center of belt to the on-axis point at the target plane and the optical axis is α whose sine has the form of $\sin\alpha=r_0/(r_0^2+z^2)^{1/2}$. In order to evaluate the difference between the intensity profile of light passing through the transparent belt and the Bessel function $J_0(k_0r\sin\alpha)$, we use the their root-mean-square error (RMSE)

$$RMSE = \sqrt{\frac{\sum_{n=1}^N \{A_n[r(n)]^2 - J_0[k_0r(n)\sin\alpha]^2\}^2}{N-1}}, \quad (S1)$$

where N is the number of sampling points in position r . If RMSE is small, the intensity profile at the target plane has a good approximation of the Bessel function. Figure 1(b) shows the dependence of the RMSE on the width Δr and radius r_0 (or $\sin\alpha$) of the belt when the propagating distance from the belt plane to the target plane is 20λ . We take $N=300$ in Fig. 1(b). We just display the cases for the RMSE smaller than 0.05, in which the good approximation can be obtained. In order to show the difference between the color and white region more straightforwardly, we select some positions, i.e. A in white region and B in color region, and plot their intensity profiles at the target plane in Fig. 1(d) and (e). When we choose the parameters $\Delta r = 1.7\lambda$ and $\sin\alpha=0.6$ at the position A in Fig. 1(b), the intensity profile has a bad approximation of Bessel function as shown in Fig. 1(d). However, for the position B with $\Delta r = 0.5\lambda$ and $\sin\alpha=0.6$, one can hardly distinguish between the intensity profile and Bessel function with its RMSE of 8.5×10^{-4} in Fig. S1(d). From Fig. 1(b), we can see the tendency that the approximation is good when the radius r_0 (or $\sin\alpha$) increases. For the belt with its width Δr smaller than the wavelength, its RMSE between the

intensity profile and Bessel function is also small enough to obtain a good approximation. If the width Δr increases, the better approximation happens at only the position in the feather-like region of Fig. 1(b). This implies that the careful weight in choosing the width of belt is required in designing a zone plate for super-resolution or super-oscillation focusing because the belt with its parameters located at the white region in Fig. 1(b) makes no sense in achieving a small spot. From this viewpoint, Figure 1(b) shows an instructive roadmap for designing a super-resolution or super-oscillation zone plate.

Interestingly, one can note that the white region in Fig. 1(b) always spreads to the position where $\Delta r = n\lambda$ ($n=1, 2, \dots$) and $\sin\alpha=1$. This phenomenon tells us a fact that light passing through the belt with the integer-wavelength width Δr and large radius r_0 has a destructive interference with the zero on-axis intensity at the center, which has no any improvement in reducing the spot size but contributing a large ring-like intensity. Therefore, for the belt with very large radius r_0 , its width should be chosen as the value with integer wavelength when one pursues a small spot at the target plane.

Correspondingly, in Fig. 1(c), we show the modulated amplitude C_n with its intensity profile having a good approximation of Bessel function. According to the conclusion derived from Fig. 1(b), we just consider the color region with the width Δr smaller than the wavelength. In this region, for a belt with the fixed width Δr , its amplitude is large for the intermediate radius r_0 (or $\sin\alpha$) and small for the low and high radius r_0 (or $\sin\alpha$), which is well consistent with the amplitude requirement for super-oscillation focusing in Fig. 2(b). This shows the advantage for zone plate to realize the super-oscillatory focusing spot with its sidelobe away from the center.

To understand the properties of light passing through a single belt, we plot the phase and amplitude profiles for the cases of the belt with different radius r_0 and fixed width $\Delta r=0.3\lambda$ in Fig. 2(d) and (e). The propagating distance is also chosen at $z=20\lambda$. The amplitude profile has the sharp variation for the small radius of the belt and the similar shape for the radius r_0 is larger than 40λ . However, the modulated amplitude $U(0)$ at $r=0$ has a peak near $r_0=20\lambda$ and slowly decreases for the large radius r_0 of the belt. For its phase profile, there is a radial (along r) phase change of π where the zero intensity happens in Fig. 2(d). Moreover, the phase also changes with the increment of the radius of the belt, which means that the phase for every spatial frequency is different. One has to choose the suitable radius r_0 of belt to make the phase difference between the neighboring frequencies become π for realizing the super-oscillation focusing, which makes the zone plate behave badly in realizing a spot with sidelobe away from the center.

2. The trust-region Newton's theory for nonlinear equations

In this paper, the numerical solution for the nonlinear problem describing the inverse problem of super-oscillation by using a zone plate or a binary-phase modulated lens system is obtained by the well-developed trust-region Newton's theory, which is the most widely used algorithm for nonlinear equations. In this section, we just show the part that has the tight relationship with our case in the paper and ignore the proof, which can be found in the relative books for more details [S1, S2], for every theory used in our codes.

Newton' theory

For most nonlinear equations with multiple variables, the basic problem can be expressed as follows:

$$\text{Given } \Gamma: \mathbf{R}^n \rightarrow \mathbf{R}^n, \text{ find } \mathbf{x}^* \in \mathbf{R}^n \text{ such that } \Gamma(\mathbf{x}^*)=0 \quad (\text{S2})$$

where Γ is assumed to be continuously differentiable. Here, in our cases, the function \mathcal{F} has the form of $\Gamma(\mathbf{v})=L(r_m)+F(r_m)+\sum_n S(v_n, r_m)C(v_n)$ for the lens system and $\Gamma(\mathbf{v})=F(r_m)+\sum_n S(v_n, r_m)C(v_n)$ for the zone plate. For simplicity, we give the solution for the problem with one variable. We can

$$\Gamma(x_0 + p) = \Gamma(x_0) + \int_{x_0}^{x_0+p} J(t)dt, \quad (\text{S3})$$

approximate the integral in Eq. (S3) by a linear term $J(x_0) \cdot p$, where $J(x_0)$ is the Jacobian of $\Gamma(x)$. Therefore, Eq. (S3) can be simplified with

$$\Gamma(x_0 + p) = \Gamma(x_0) + J(x_0)p, \quad (\text{S4})$$

Now, we can solve the step p that makes $\Gamma(x_0+p)=0$, which gives the Newton iteration for this problem. The solution is

$$\Gamma(x_0) = -J(x_0)p, \quad (\text{S5})$$

$$x_1 = x_0 + p. \quad (\text{S6})$$

From Eq. (S5) and (S6), one can see that the choice of step p is very important in solving the nonlinear problem successfully. Many methods has been developed to find the suitable step p for the various nonlinear problem. The trust-region method is the most popular one for its global convergence properties and rapid local convergence with exact solution.

Trust-region method

As shown in Eq. (S4), the step p is a root of the $\Gamma(x_0+p)=0$. Equivalently, the step p is also a minimum of the Euclidean norm $m(p)$

$$\begin{aligned} m(p) &= \frac{1}{2} \|\Gamma(x_k + p)\|_2^2 = \frac{1}{2} \|\Gamma(x_k) + J(x_k)p\|_2^2 \\ &= \frac{1}{2} \Gamma(x_k)^T \Gamma(x_k) + p^T J(x_k)^T \Gamma(x_k) + \frac{1}{2} p^T J(x_k)^T J(x_k)p \end{aligned}, \quad (\text{S7})$$

where the sign $\|\cdot\|_2^2$ stands for the Euclidean norm and the s^T is the transpose of the matrix s .

Hence, the subproblem of trust-region method is to find the minimum of function $m(p)$ in the limited region $\|p\| \leq \Delta_k$, where Δ_k is the trust-region radius which has the positive value. Choosing the trust-region radius Δ_k at each iteration is the first problem that should be settled down in building the trust-region method. We follow the general way for evaluating the trust-region radius by the agreement between the model function $m(p)$ and the objective function $\Gamma(x_k)$ at the previous iterations. For the iteration with its step p_k , we can use the ratio

$$\rho_k = \frac{\|\Gamma(x_k)\|_2^2 - \|\Gamma(x_k + p_k)\|_2^2}{m_k(0) - m_k(p_k)}, \quad (\text{S8})$$

where the numerator and denominator evaluate the actual and predicted reduction. Because the

step is obtained by minimizing the $m(p)$ over the region includes $p=0$, the denominator always has the nonnegative value. This implies that, if the ratio ρ_k is negative, the next objective value is larger than the current value $\Gamma(x_k)$. Moreover, when ρ_k is close to 1, it is the good agreement for this step, resulting that it is safe to use the trust region of this step in the next iteration. However, when ρ_k is very small (close to zero) or negative, we should decrease the radius of trust region. When we carry out this method in a computer code, its flowchart for the trust-region method has the form as Fig. S1.

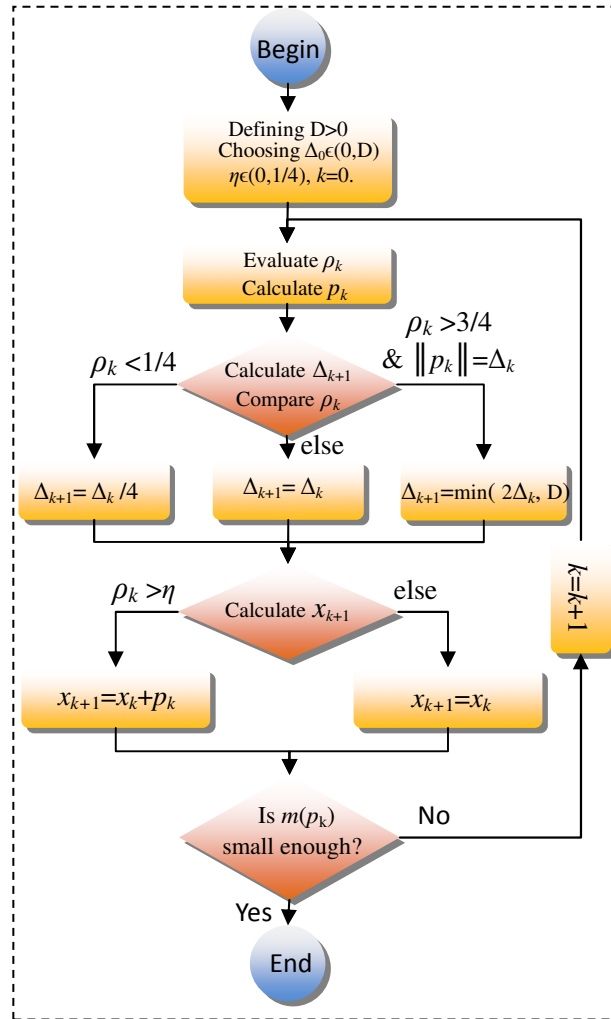


Figure S1 | The flowchart of the trust-region method based on the Newton's theory for non-linear equations.

In the flowchart, the calculation of p_k is usually carried out by using the dogleg algorithm, which is a quick and efficient method for p_k . Next, we introduce the dogleg algorithm.

Dogleg algorithm

To obtain the approximate solution p of $\min[m(p)]$ in Eq. (S7), we use the dogleg algorithm which is based on the Cauchy point p_k^C and the unconstrained minimizer p_k^J . The Cauchy point is used to quantify the sufficient reduction of p_k for global convergence proposes. The Cauchy point is

$$p_k^C = -\tau_k \left(\Delta_k / \|J_k^T \Gamma(x_k)\| \right) J_k^T \Gamma(x_k), \quad (\text{S9})$$

where

$$\tau_k = \min \left\{ 1, \|J_k^T \Gamma(x_k)\|^3 / [\Delta_k \Gamma^T(x_k) J_k (J_k^T J_k) J_k^T \Gamma(x_k)] \right\}. \quad (\text{S10})$$

To realize the curved trajectory needed in dogleg algorithm for quick convergence globally, the unconstrained minimizer p_k^J is introduced. When the Jacobian J_k has full rank, the $m_k(p)$ has the unique minimizer. Therefore, the unconstrained minimizer is the good approximation for obtaining the solution of $\min[m(p)]$. The unconstrained minimizer has the form of

$$p_k^J = -J_k^{-1} \Gamma(x_k). \quad (\text{S11})$$

In the practical implementation of dogleg algorithm, the Cauchy point and the unconstrained minimizer are combined together for determining the approximate solution p of $\min[m(p)]$. The flowchart of dogleg algorithm is shown in Fig. (S2).

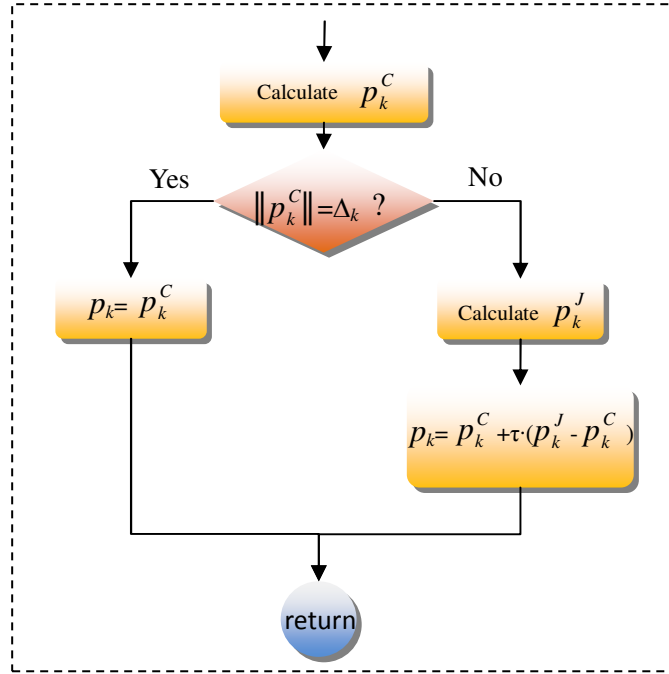


Figure S2 | The flowchart of dogleg algorithm for solving the subproblem in trust-region Newton method

3. Construct a super-oscillatory focused spot by focusing the light with rigorous single spatial frequencies

We have showed the generation of a super-oscillatory spot by using a zone plate and a binary-phase-base lens system. Here, to investigate the properties of the super-oscillatory focusing in optics, we construct an optical super-oscillatory pattern by interfering the light of different spatial frequencies with modulated amplitudes to display how the super-oscillation in optical focusing happens. For the focusing of a unpolarized beam with the single spatial frequency, it can be approximated by the scalar Debye theory [S3, S4]. The electric field at the focal plane is proportional to

$$U(r, \theta) = \int_0^{2\pi} \exp(i\mathbf{k} \cdot \mathbf{r}) d\varphi = \int_0^{2\pi} \exp[ik_0 \sin \alpha \cdot r \cos(\varphi - \theta)] d\varphi = 2\pi i \cdot J_0(k_0 r \sin \alpha), \quad (\text{S12})$$

where $k_0=2\pi/\lambda$. Without loss of generality, we consider the interference of light with N different spatial frequencies whose amplitudes are modulated. Following the results in Eq. (S12), the total electric field after interference can be expressed as

$$f(r) = \sum_{n=1}^N C_n J_0(k_0 r v_n), \quad (\text{S13})$$

where C_n and v_n are the modulated amplitude and the corresponding NA of n -th spatial frequency, respectively. First we show the simplest case of $N=2$ which is shown in Fig. S3(a). According to the results in Fig. 4, if the super-oscillation happens, the first zero-intensity position in the total electric field f after interference should be located at $r < r_s$. In Fig. S3(a), the first zero-intensity position is chosen at $r=r_0$. Then the zero intensity at $r=r_0$ can be realized by adjusting the amplitudes of f_1 and f_2 . Here, we suggest a set solution of $C_1=2.2041$ and $C_2=-1.2041$, where the negative amplitude can be achieved by introducing a phase retardation of π in optics. The total electric field f seems to be the result that one pulls down the electric field f_1 of the maximum spatial frequency along the chromatic zone in Fig. S3(a) until the zero electric field (or completely destructive interference) occurs at r_0 . When the pulling down of f_1 continues, the arbitrarily small super-oscillatory spot can be obtained only if the on-axis intensity at $r=0$ is nonzero, which gives the reason for the fact that it is possible to theoretically get a super-oscillatory spot with infinitesimal size [S5, S6]. Another consequence of pulling down f_1 is the further decrement of first valley with negative value that leads to the increment in intensity of high sidelobe as shown in Fig. S3(a), which can explain why the super-oscillation always accompanies with a high sidelobe [S5, S6]. From the case displayed in Fig. S3(a), we claim that, the super-oscillation in optics is the fact that the completely destructive interference happens at the some points with the neighboring interval smaller than the super-oscillation criterion r_s . The case in Fig. S3(a) shows the simplest prototype that represents the inverse problem of super-oscillation: what is the amplitude for every spatial frequency if one wants to realize the nonzero intensity at $r=0$ and the zero intensity at $r=r_0$ by using two given spatial frequencies.

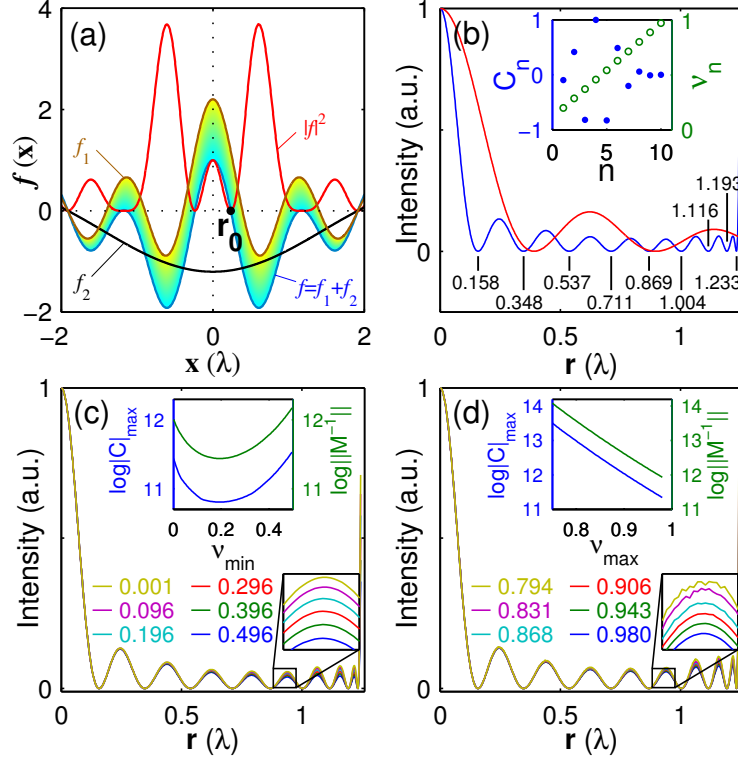


Figure S3 | The constructed optical pattern by inverse problem of super-oscillation. (a) The constructed super-oscillation by the light with two frequencies whose electric fields at the interfered area are $f_1=2.041J_0(0.98k_0r)$ and $f_2=-1.041J_0(0.2k_0r)$, respectively. **(b)** The intensity profiles of the constructed super-oscillation (blue) pattern by interference of the light with 10 spatial frequencies and the optical pattern (red) from the maximum frequency. Inset: the values of 10 given spatial frequencies (hollow circle) with equal interval and the solved \mathbf{C} (solid dot) with the normalized value. **(c)** The intensity profiles of constructed super-oscillatory pattern when the minimum spatial frequency v_{\min} is changing in the range of $[0.001, 0.496]$ but the maximum spatial frequency v_{\max} is fixed to 0.98. Inset: the maximum in the absolute value of the solved \mathbf{C} (blue) and the corresponding norm $\|\mathbf{S}^{-1}\|$ (green) vs the different v_{\min} . **(d)** The intensity profiles of constructed super-oscillatory pattern when v_{\max} is changing in the range of $[0.75, 0.98]$ but v_{\min} is fixed to 0.01. Inset: the maximum in the absolute value of the solved \mathbf{C} (blue) and the corresponding norm $\|\mathbf{S}^{-1}\|$ (green) vs the different v_{\max} .

Next, we discuss the inverse problem of super-oscillation generally. Assuming that we want to realize the electric field $\mathbf{F}=[f_1, f_2, \dots, f_M]^T$ at the prescribed position $\mathbf{r}=[r_1, r_2, \dots, r_M]^T$ by using the interference of light from the given spatial frequencies $\mathbf{v}=[v_1, v_2, \dots, v_N]^T$, the problem of determining the unknown amplitude $\mathbf{C}=[C_1, C_2, \dots, C_N]^T$ can be expressed by

$$\mathbf{S}\mathbf{C}=\mathbf{F}, \quad (\text{S14})$$

where \mathbf{S} is an $M \times N$ matrix that has its matrix element $S_{mn}=J_0(k_0r_m v_n)$ according to Eq. (S13). Because the only unknown variable in Eq. (S14) is \mathbf{C} , it is a simple linear-equation problem to solve \mathbf{C} , whose solution exists if $N \geq M$. For simplicity, here we just discuss the case of $N=M$ which implies that \mathbf{S} is a square matrix. In this case, if \mathbf{S} is invertible or has the nonzero determinate, which means the \mathbf{S}^{-1} is not a singular matrix, \mathbf{C} has the only solution of $\mathbf{C}=\mathbf{S}^{-1}\mathbf{F}$. For a

given \mathbf{F} , \mathbf{S}^{-1} is the key parameter that determines the cost \mathbf{C} for super-oscillation. Therefore, we can use the norm $\|\mathbf{S}^{-1}\|$ to evaluate the cost of super-oscillation. The norm $\|\mathbf{S}^{-1}\|$ depends on the prescribed position \mathbf{r} and the spatial frequency \mathbf{v} . A fast super-oscillation means that the interval $\Delta r=r_{m+1}-r_m$ is very small. The m and $m+1$ row of \mathbf{S} tends to have little difference so that \mathbf{S} has its determinate $|\mathbf{S}|$ close to zero, which leads to the very large norm $\|\mathbf{S}^{-1}\|$ that causes a high cost in amplitude \mathbf{C} . Therefore, the faster super-oscillation always requires the higher cost.

Then, using the inverse problem of super-oscillation demonstrated above, we show an example that realizes a super-oscillatory spot with its high sidelobe away from center for super-resolution focusing. As shown in Fig. S3(b), for the $N=10$ given spatial frequencies $\mathbf{v}=[v_{\min}, v_{\min}+\Delta v, \dots, v_{\min}+(N-2)\cdot\Delta v, v_{\max}]$ with equal frequency interval $\Delta v=v_{\max}-v_{\min}/(N-1)$ where $v_{\min}=0.201$ and $v_{\max}=0.98$, our aim is to use the frequencies \mathbf{v} to realize a customized super-oscillatory pattern with its intensity profiles obeying $\mathbf{F}=[1, 0, \dots, 0]^T$ at the prescribed position $\mathbf{r}=[0, 0.158\lambda, 0.348\lambda, \dots, 1.233\lambda]$. According to Eq. (S14), we can provide the solution \mathbf{C} that is shown in the inset of Fig. S3(b). Using Eq. (S13) and the solved \mathbf{C} by the inverse problem of super-oscillation, the intensity profile of constructed super-oscillatory pattern is displayed in Fig. S3(b). The constructed pattern indeed oscillates faster than the optical pattern from the maximum frequency. More importantly, the sidelobe in the constructed pattern is pushed several wavelengths away from the super-oscillatory main spot at the center by artificially padding the zero-intensity position between the sidelobe and main spot when setting the targeted \mathbf{F} in practical application. In the intermediate area between the sidelobe and main spot, the zero intensity is used to suppress the high intensity of sidelobe so that the sidelobe has to move away from the center. The distance between the sidelobe and main spot can be enlarged by introducing more zero-intensity locations in their intermediate region, which implies more cost in the corresponding amplitude \mathbf{C} [S7]. Nevertheless, this method provides an unrestricted route in theory for realizing a super-oscillatory focusing spot with its sidelobe arbitrarily far away from the center, which is a significant promotion in popularizing the super-oscillation in super-resolution imaging. Interestingly, the solved amplitude \mathbf{C} has the alternating sign of positive or negative with its amplitude module small for low and high spatial frequencies and large for the intermediate spatial frequencies.

It is not the sole solution \mathbf{C} for realizing the super-oscillatory pattern with the customized intensity \mathbf{F} at the prescribed position \mathbf{r} shown in Fig. S3(b) when we change the given spatial frequencies \mathbf{v} . In Fig. S3(c), we fix the maximum spatial frequency v_{\max}/λ to be $0.98/\lambda$ and change v_{\min} from 0.01 to 0.496, so that the $N=10$ given spatial frequencies have the form of $\mathbf{v}=[v_{\min}, v_{\min}+\Delta v, \dots, v_{\min}+(N-2)\cdot\Delta v, v_{\max}]$ with equal frequency interval $\Delta v=v_{\max}-v_{\min}/(N-1)$ where v_{\min} is changing and $v_{\max}=0.98$. According to the inverse problem described by Eq. (S14), we display the intensity profiles of some solutions in Fig. S3(c) that has absolutely the same intensity \mathbf{F} at the prescribed position \mathbf{r} although a little deviation between different frequency groups exists at the unprescribed position. It is worthy to note that both the norm $\|\mathbf{S}^{-1}\|$ and the maximum absolute value $|\mathbf{C}|_{\max}$ in every case experience a valley near $v_{\min}=0.2$ when v_{\min} varies from 0.01 to 0.496. This reveals that the cost for every frequency group is different and an optimal solution is existent in our case, which is an undeniable proof that the optimization mechanism of super-oscillation is considerably developed by choosing the suitable spatial frequencies. The existence of the optimal solution for super-oscillation renovates the cognizance that there is no cheapest band-limited function for super-oscillation [S7]. Furthermore, we use the fixed $v_{\min}=0.01$ and varied v_{\max} from

0.75 to 0.95 to generate the spatial frequency group \mathbf{v} with equal frequency interval $\Delta v = v_{\max} - v_{\min} / (N-1)$. Likely, the customized intensity \mathbf{F} at the prescribed position \mathbf{r} is also achieved and shown in Fig. S3(d). In this case, the cost of super-oscillation exponentially decreases with the increment of v_{\max} , which implies that the high spatial frequency is preferred in optimizing the super-oscillation with the smallest cost.

4. Parameters of binary phase mask in Fig. 3b

Table S1. Data of designed binary phase in Fig. 3b

n	$\sin\theta_n$	n	$\sin\theta_n$
0	0	16	0.5196
1	0.0317	17	0.5517
2	0.0635	18	0.5835
3	0.0955	19	0.6154
4	0.1291	20	0.647
5	0.1614	21	0.6796
6	0.1941	22	0.7113
7	0.2271	23	0.7435
8	0.2602	24	0.7742
9	0.2928	25	0.8063
10	0.3247	26	0.8357
11	0.3576	27	0.8676
12	0.3899	28	0.8949
13	0.4222	29	0.9244
14	0.4544	30	0.95
15	0.487		

References

- [S1] Dennis, J.E. and Schnabel, R.B. Numerical methods for unconstrained optimization and nonlinear equations (Prentice-Hall, Inc, New Jersey, 1983).
- [S2] Nocedal, J. and S. J. Wright. Numerical Optimization, Second Edition. (Springer Series in Operations Research, Springer Verlag, 2006).
- [S3] Debye, P. "Der Lichtdruck auf Kugeln von beliebigem Material". *Annalen der Physik* **335**, 57-136(1909).
- [S4] Min Gu, Advanced Optical Imaging Theory, 75 (Springer-Verlag, New York, 1999).
- [S5] Rogers E. T. F., Lindberg J., Roy T., Savo S., Chad J. E., Dennis M. R., & Zheludev N. I., "A super-oscillatory lens optical microscope for subwavelength imaging." *Nature Mater.* **11**, 432-435 (2012).
- [S6] Huang F. M. & Zheludev N. "Super-Resolution without Evanescent Waves." *Nano Lett.* **9**, 1249-1254 (2009).
- [S7] Kempf. A. & Ferreira, P. J. S. G., S. "Unusual properties of superoscillating particles". *J. Phys. A* **37**, 12067-12076 (2004).